ORIGINAL ARTICLE

Sub-switching domain effect for analysis the non-linear dielectric behavior of $(K_{0.49} Na_{0.49}Li_{0.02}) (Nb_{0.98}Sb_{0.02})O_3$ ceramic based on Rayleigh model

Ibrahim A. Atito[1] · **H. T. Shaban[2]** · **A. Salem[2]** · **Mohammed Ezzeldien[3]** · **Abd El-razek Mahmoud[1]**

Abstract

The solid-state sintering technique has been implemented to synthesize $(K_{0.5}Na_{0.5}NbO_3)$-0.02(LiSbO_3) (KNN-LS) Pb-free ceramic. The crystal structure, dielectric and ferroelectric properties of the prepared material were investigated. Pure orthorhombic perovskite phase $[I_{(220)}/I_{(002)} = 1.68]$ with Amm2 space group has been detected at room temperature for sintered ceramic. Two anomalous permittivity peaks corresponding to orthorhombic–tetragonal (O–T) phase transition at $T = 175$ °C and tetragonal–cubic (T–C) phase transition at $T = 355$ °C have been observed. At polymorphic phase transition, the Rayleigh model shown the extrinsic contributions caused by domain wall motion is about 80%, while the intrinsic contribution attributed to the lattice distortion is about 20%. Ferroelectric properties were investigated in a wide range of temperatures (RT-225)°C. The results shown a conductive material at high temperature due to the higher cation disorder and leakage current above PPT. The present results are interested for understanding the mechanism of t permittivity–temperature behavior of KNN-doped LS ions based on Rayleigh model. The large remnant polarization and low coercive field below PPT make the material a suitable candidate for energy storage application.

Keywords Lead-free ceramics · Polymorphic phase transition · Rayleigh analysis · Leakage current

1 Introduction

Ferroelectric ceramic materials are widely used in several electronic applications, such as sensors, actuators, and transducers [1–7]. Owing to the environmental restrictions on lead-based materials and their high toxicity, (K_{1-x},Na_x) NbO_3 has drawn much attention as promising lead-free candidates materials instead of lead-based such as PZT due to its excellent performance [8–12]. When $x = 0.5$, the system

shown an outstanding piezoelectric property due to form morphotropic phase boundary (MPB) as a contributed to orthorhombic–tetragonal phase coexistence or a combination $KNbO_3$ ferroelectric with $NaNbO_3$ anti-ferroelectric at room temperature. Furthermore, it has a high Curie temperature > 400 °C which makes the material as a suitable candidate for a piezoelectric applications in a wide range of temperature [13]. However, the volatilization of alkali components at high sintering temperature is the most drawback of this system [14]. Therefore, several numbers of researches have been paid attention to improve the functional properties and sinterability of KNN to be more applicable as piezoelectric materials. The enhancement procedures are doping the material with ferroelectric materials, such as $BaTiO_3$, $(Bi,Na)TiO_3$ [15], $SrTiO_3$ [16], etc., non-ferroelectric materials, such as $LiNbO_3$, $LiTaO_3$, LiSbO3 [16]. Moreover, the shift of the polymorphic phase transition (PPT) to near room temperature has resulted in a significant improvement in dielectric and piezoelectric characteristics [17]. In general, the dielectric and piezoelectric responses are almost always non-linear and hysteretic behavior. It is well understood, dielectric activity can be generally conducted by

✉ Ibrahim A. Atito
ibrahim94@sci.svu.edu.eg

Abd El-razek Mahmoud
abdelrazek.mahmoud@sci.svu.edu.eg

[1] Piezoelectric and Ferroelectric Measurements Lab, Physics Department, Faculty of Science, South Valley University, Qena 83523, Egypt

[2] Physics Department, Faculty of Science, South Valley University, Qena 83523, Egypt

[3] Metallurgy and Material Science Test (MMST) Lab, Physics Department, Faculty of Science, South Valley University, Qena 83523, Egypt

intrinsic and extrinsic contributions; the intrinsic contribution demonstrates the dielectric response due to lattice distortion and domain wall propagation, which always reversible when applying external electric fields. On the other hand, the extrinsic contribution, might be attributed to the reversible or irreversible movement of the domain walls or phase boundaries motion [18, 18–21]. However, near $T_{O–T}$ dielectric properties have several limitations, such as excessive temperature influence of piezoelectric characteristics, which is a major drawback for commercial applications. Understanding the dielectric response at polymorphic phase transitions is critical for improving the thermal stability of KNN-based ceramics. Furthermore, few studies that have a considerable impact on their practical applications have been conducted. As a result, additional investigation is required. To solve the previous issues, the Rayleigh model is being used in the domain's sub-switching region. Furthermore, Rayleigh law has been applied in textured KNN ceramics with high level of parallels to the external electric field and the results reported increased the dielectric response due to lattice deformation effect [22]. Recently, Bin Peng et al. evaluate domain wall motion in $(K_{0.5}Na_{0.5})NbO_3$ during polymorphic phase transition [23]. On the other hand, whereas ferroelectric materials offer a wide variety of uses in energy inter-conversion based on the ease with which the polarization and coercive field may be changed with temperature. The present work introduces an overview for understanding the dielectric nonlinearity mechanism of KNN-LS ceramic using the Rayleigh model at sub-coercive electric fields and extract the dominant contribution of intrinsic and extrinsic value to dielectric characteristics near polymorphic phase transitions (PPT). Furthermore, mechanisms on ferroelectric properties in the over wide range of temperatures were investigated.

2 Experimental procedures

2.1 Preparation and characterization

The $0.98\ K_{0.5}Na_{0.5}NbO_3$-$0.02LiSbO_3$ (abbreviated as KNLNS) ceramics were fabricated via the conventional solid-state reaction method. For 12 h, the raw materials K_2CO_3 (99%), Na_2CO_3 (99.8%), Nb_2O_5 (99.5%), Li_2CO_3 Sb_2O_5 (99.99%) were ball-milled. The mixture was dried and calcined at 850 °C for 2 h. The calcined powders were then uniformly crushed into pellets with a diameter of 10 mm and a thickness of 1–1.5 mm. The powders were then thoroughly mixed with polyvinyl alcohol (binder) and granulated to obtain a harmonious mixture to proceed with the sintering. At 1090.0C for 3 h with a heating rate of 5 °C/min, the pressed pellets were sintered to air and then cooled to room temperature at 5 °C/min. In the air, all calcination and

sintering steps were carried out. The compositional crystal structure was examined at an angle of two thetas from 20° to 70°, using an X-ray diffractometer(XRD) (Philips diffractometer PW 3020) with monochromatic CuKα ($T = 1.54178$ Å). The microstructure was observed using a scanning electron microscope (SEM, JEOL JSM- 5500LV, scanning microscope JEOL). Electrical characterizations were performed using silver electrodes that fired at 850 °C for 30 min. The dielectric sample measurements were performed using the LCR meter as a function of frequency and temperature. The ferroelectric properties estimated by the P–E loop of sintered ceramic were measured at a wide range of temperatures (RADIANT Precision Premium II Multiferroic Ferroelectric Test System 10 kV HVI-SC Model 609B) Ferroelectric measurement system.

3 Results and discussion

3.1 Phase structure and microstructure properties

The room temperature patterns of X-ray diffraction (XRD) for (0.98) $[(K_{0.5}Na_{0.5})NbO_3]$–0.02 $LiSbO_3$ calcined powder and sintered ceramic were performed and the patterns were displayed into Fig. 1. As observed, a pure perovskite structure with no obvious any track for secondary phase or additional peaks into calcined powder pattern within the detectable limit of the XRD, indicates that 0.02 LS has diffused successfully entirely the KNN lattice to form KNN-LS solid solution. The diffraction peaks were cited from KNN with orthorhombic symmetry (PDF# 71-0946) and (Amm2) space group. As it is well known, the ionic radius of Li^+ (1.23 Å) is very close to the ionic radius of Na^+ (1.39 Å) and, K^+ (1.6 Å), so it is suitable to occupy the A site of KNN lattice, while the ionic radius of Sb^{5+} is (0.6 Å) is very close to the ionic radius of Nb^{5+} (0.69 Å), so it is suitable to occupy the B site of KNN lattice [2]. The Bragg reflections of the sintered ceramic at 1080 °C/2 h shown the same pattern of calcined powder indicate the thermal stability of compound at high sintering temperature. A complete solid solution with pure perovskite phase and orthorhombic structure was attributed to the low melting points of Li_2CO_3 (723 °C), and Sb_2O_5 (380 °C) make the KNN–LS ceramics form a complete solid solution with pure perovskite phase and orthorhombic structure. To investigate the effect of Li^+, Sb^{+5} ions and thermal processing calcination/sintering conditions have any influence on the orthorhombic/tetragonal structure of KNN, we can use the following formula (Eqs. 1, 2).

$$\varphi_{\text{Orthorhombic}} = \frac{\left(\frac{I_{110}}{I_{001}} + \frac{I_{220}}{I_{002}}\right)}{2},\tag{1}$$

Fig. 1 Room temperature X-ray diffraction patterns of KNN-LS sintered ceramic
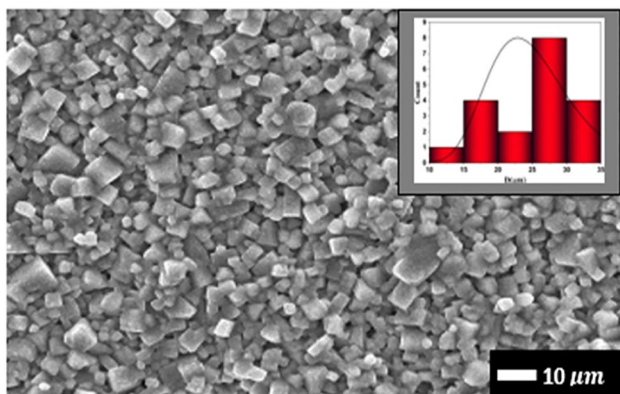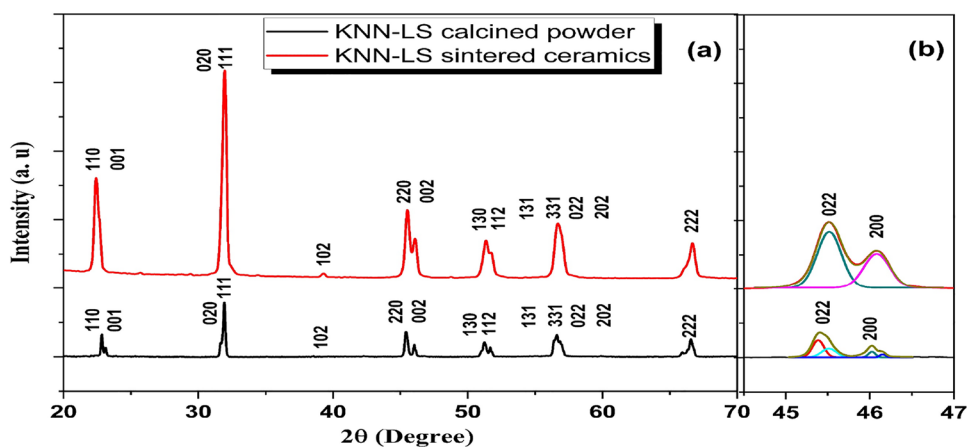

Fig. 2 Sem micrograph of KNN-LS ceramics

$$\varphi_{\text{Tetragonal}} = \frac{\left(\frac{I_{001}}{I_{100}} + \frac{I_{002}}{I_{220}}\right)}{2}, \tag{2}$$

where I_{hkl} represents the intensity of the corresponding peaks (hkl), and the ratio φ is estimated to be 1.7 for pure orthorhombic phase and 0.53 for tetragonal phase[24]. The equation shown the φ value is 1.85 for KNN-LS powder and 1.7 for sintered ceramics which reveal that the KNN-LS modulate its orthorhombicity by sintering processing. Figure 1(b) shows the de-convolution patterns between (45 and 47) of peak positions to clarify the results of Eq. 1. The de-convolution of peaks shown in fig. b forms only single orthorhombic phase at sintered pattern, while the calcined powder shown presents two orthorhombic phases existence to each other which refer to high φ value at calcined powder. Figure 2 shows the SEM image of the KNN-LS sintered ceramic at 1080 °C/2 h. The morphology showing the grain boundary size of KNN-doped 0.02LS is lower than the grain

boundary size of pure KNN [25] could be owing to the lower ionic radius of Li and Sb ions comparable to the ionic radius of Na, K and Nb ions which prohibit materials for grain growth process. The lower grain boundary is contributed in decreasing the sintering temperature from 1100 °C for pure KNN [26] to 1080 °C for the present sample. Furthermore, lower melting point of Li_2O_3 720 °C and melting point of Sb_2O_5 is 380 °C can also responsible for reducing the sintering temperature of KNN. Therefore, when the sintering temperature decreased, it could not provide the enough energy for the grain growth process. The obvious liquid phase and porosity exist into grain boundary are due to Na_2O volatilization during the sintering process lead to a deviation from stoichiometry phase and porosity exist into grain boundary are due to Na_2O volatilization during the sintering process lead to a deviation from stoichiometry.

The analysis on the grain size distributions of KNN-LS ceramics is shown in Fig. 5. The average grain size of pure KNN ceramics is approximately 2.26 µm [27], which were calculated using the grain size distribution. On the other hand, the average grain size of KNN-LS ceramics is 2.2 µm and grain growth is typically dependent on grain boundary mobility; however, the pores are the most important factor influencing grain boundary mobility.

3.2 Dielectric properties

The temperature dependence of permittivity for KNN-LS sintered ceramic at 1080 °C/2 h measured at different frequencies (1, 100, and 1000 kHz) is shown in Fig. 3. In agreement with the previously reported works, the permittivity vs. temperature curve is revealed two anomalies permittivity peaks corresponding to orthorhombic
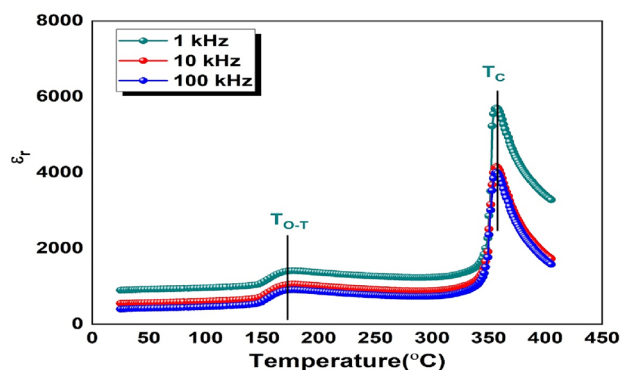
Fig. 3 Dependence of dielectric constant (ε) on temperature (measured at 10,100 and 1000 kHz) for KNLNS ceramics

to tetragonal phase transition at lower temperature ($T_{O–T} = 175$ °C) and tetragonal–cubic phase transition at higher temperature ($T_{T–C} = 355$ °C). The relative decreasing of phase transition temperatures values compared to pure KNN are attributed to that as previously reported [26], Nb^{5+} with Sb^{5+} reduces Tc.

3.3 Rayleigh analysis

The dielectric response in ferroelectric materials usually nonlinear under external electric field can be adequately described using Rayleigh relations Eqs. (3, 4) [28, 29] at sub-switching of domain at low amplitude of electric. The Rayleigh model assumed that dielectric activity can be divided into intrinsic and extrinsic contributions, where the intrinsic contribution reflects the lattice distortion or domain wall propagation, while the extrinsic contribution can be ascribed to the domain wall displacement and as consequently the domain grows.

$$P = \varepsilon_0 \cdot \left[\left(\varepsilon'_{\mathrm{int}} + \alpha \cdot E_0 \right) \cdot E \pm \left(\frac{\alpha}{2} \right) \cdot \left(E_0^2 - E^2 \right) \right], \quad (3)$$

$$\varepsilon'_r \left(E_0 \right) = \varepsilon'_{\mathrm{init}} + \alpha \cdot E_0, \quad (4)$$

where E is the applied electric field corresponding to maximum amplitude E_0, P refers to the polarization under the applied electric field. The coefficient $\varepsilon'_{\mathrm{init}}$ represents the intrinsic contribution of dielectric response and α the Rayleigh coefficient. Irreversible domain wall mobility or extrinsic coefficient is denoted by αE_0 [28, 29]. Figure 4 shows the '(P–E) hysteresis loops' in a series amplitude of electric field (2–6 kV/cm) in the wide range of temperature (RT–225 °C). All hysteresis loops can be well fitted by Rayleigh Eq. (4),

where the permittivity increased with increasing the applied electric field. Figure 5 depicts the dielectric permittivity $\varepsilon'(E_0)$ dependancey on electric field at different temperatures. The figure revealed an essentially linear relationship of permittivity as a function of electric field and both of intrinsic and extrinsic coefficients can be obtained from these relation, Furthermore, to clarify the largest dielectric response of the present ceramic at polymorphic phase transition point, the changes of reversible and irreversible coefficients corresponding to temperature have been displayed into Fig. 6.

The results indicate that the temperature strongly influences the intrinsic and extrinsic values during both the orthorhombic phase and the polymorphic phase transition (PPT). The irreversible coefficient α caused by domain wall motion is increased with temperature and possess the maximum value at 175 °C. When the sample heated above $T_{O–T}$, the α value declines significantly and possesses the minimum value around 200 °C, this behavior is attributed to the clamping effect which grow in the tetragonal phase [23], In addition, there are two factors related to domain walls that influence the irreversible response: domain wall mobility and domain wall density. Moreover, a large number of the domain walls may reduce the domain wall mobility, which may counteract the effect of the domain wall density [28, 30], Furthermore, lattice distortion and internal stress may increase during the polymorphic phase transition, and the number of domain walls may increase to minimize the internal stress, as a result, the α magnitude reduces dramatically. In contrast, the initial permittivity reaches the maximum at 200 °C. Figure 6(a) also demonstrates that above 200 °C, the initial permittivity decreases dramatically as the temperature rises, which is ascribed to the increase in domain wall density [30], which reduces spontaneous distortion. In contrast, we can see that as the temperature rises, the Rayleigh coefficient rises again; this is because the temperature is adequate to enhance the mobility of the domains (as we know that the domain walls are thermally activated). However, the increase is not significant because of the large number of domain walls, which clamp the mobility of domains. Figure 6(b) refers to the terms $\alpha.E_0 / \varepsilon'(E_0)$ and $\varepsilon_{\mathrm{init}}(E_0) / \varepsilon'(E_0)$ which are calculated to determine the ratio of the intrinsic contribution from the reversible lattice distortion and extrinsic contributions from the irreversible domain wall movement to the total dielectric response. As shown in Fig. 6(b), the ratio $\alpha.E_0 / \varepsilon'(E_0)$ represents about 80% of the total permittivity at PPT. Once the temperature rises above 175 °C, the domain wall mobility may decrease due to the increasing domain wall density during polymorphic phase transition, which also results in a decrease in the α value and the

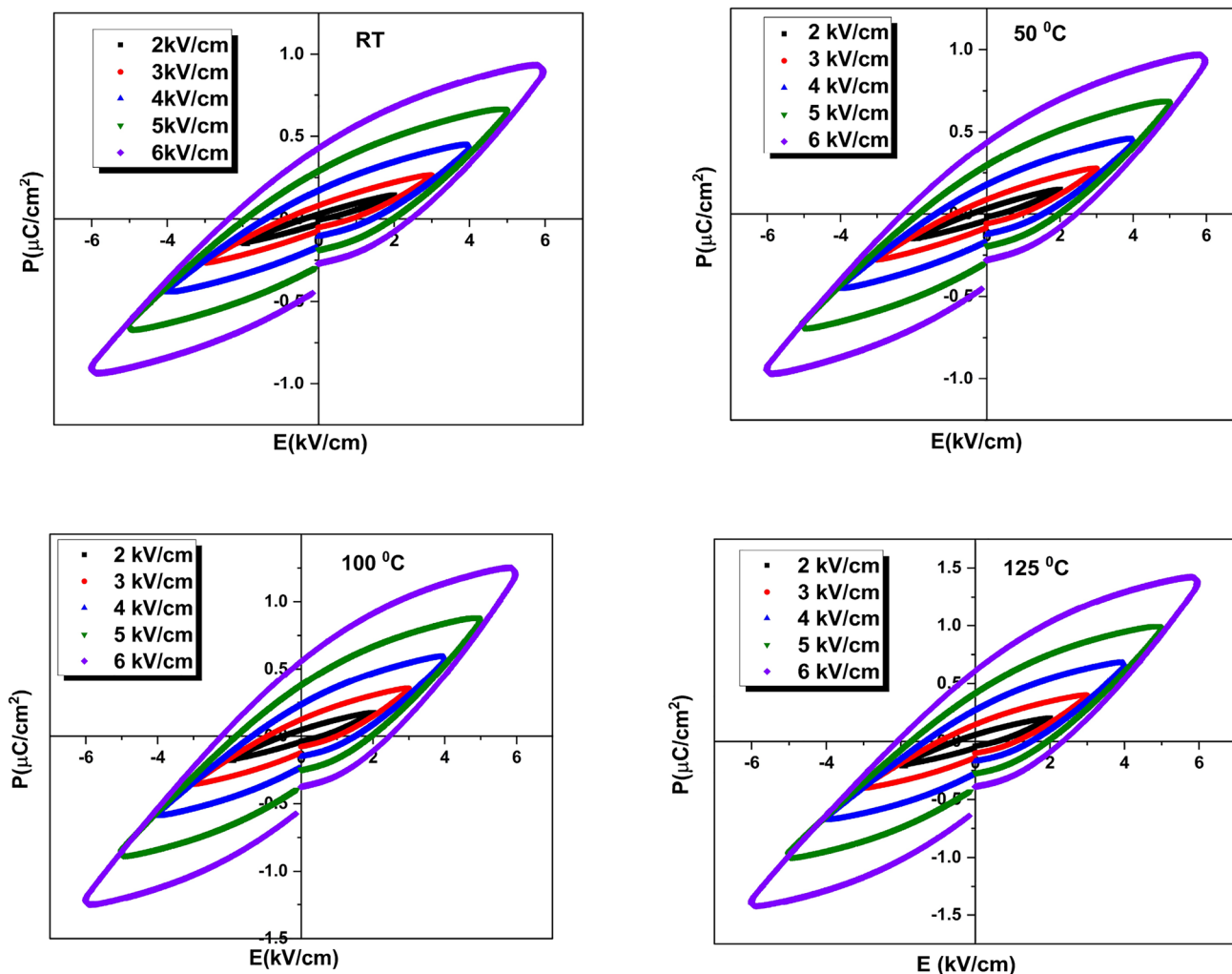**Fig. 4** The typical measured and calculated P–E hysteresis loops for KNLNS ceramics during a wide range of temperatures

ratio $\alpha.E_0/\varepsilon'(E_0)$. On the other hand, the ratio $\varepsilon_{init}(E_0)/\varepsilon'(E_0)$ represents about 20% from the total permittivity. As a result, the irreversible domain wall motion is the major contributor at the coexistence point between orthorhombic and tetragonal phases (PPT).

3.4 In-situ Ferroelectric characterization at switching region

One of the most essential components in current applications, such as sensors, electronic devices, and energy storage, is to investigate the ferroelectric characteristics at a wide range of temperatures to enhance the thermal stability. Figure 7 shows the polarization and current-dependent electric field of KNN-LS sintered ceramic at various temperatures (RT-225 °C). The polarization and current hysteresis loops show normal ferroelectric loop from RT up to PPT temperature (175 °C), then a conductive P–E loop combined with high conductivity current has been conducted at high temperature > 175 °C. The maximum current value into (I–E) loop corresponding to coercive field (E_c) is attributed to the domain switching contribution [31]. Decreasing the remnant polarization with temperature might be owing to disturbance of the atoms from their equilibrium positions and as consequently increasing the degree of cations disorder. Furthermore, increasing the thermal activation leads to pinshed the ferroelectricity and as consequently decrease the P_r value at high temperature. The decreasing into E_c value
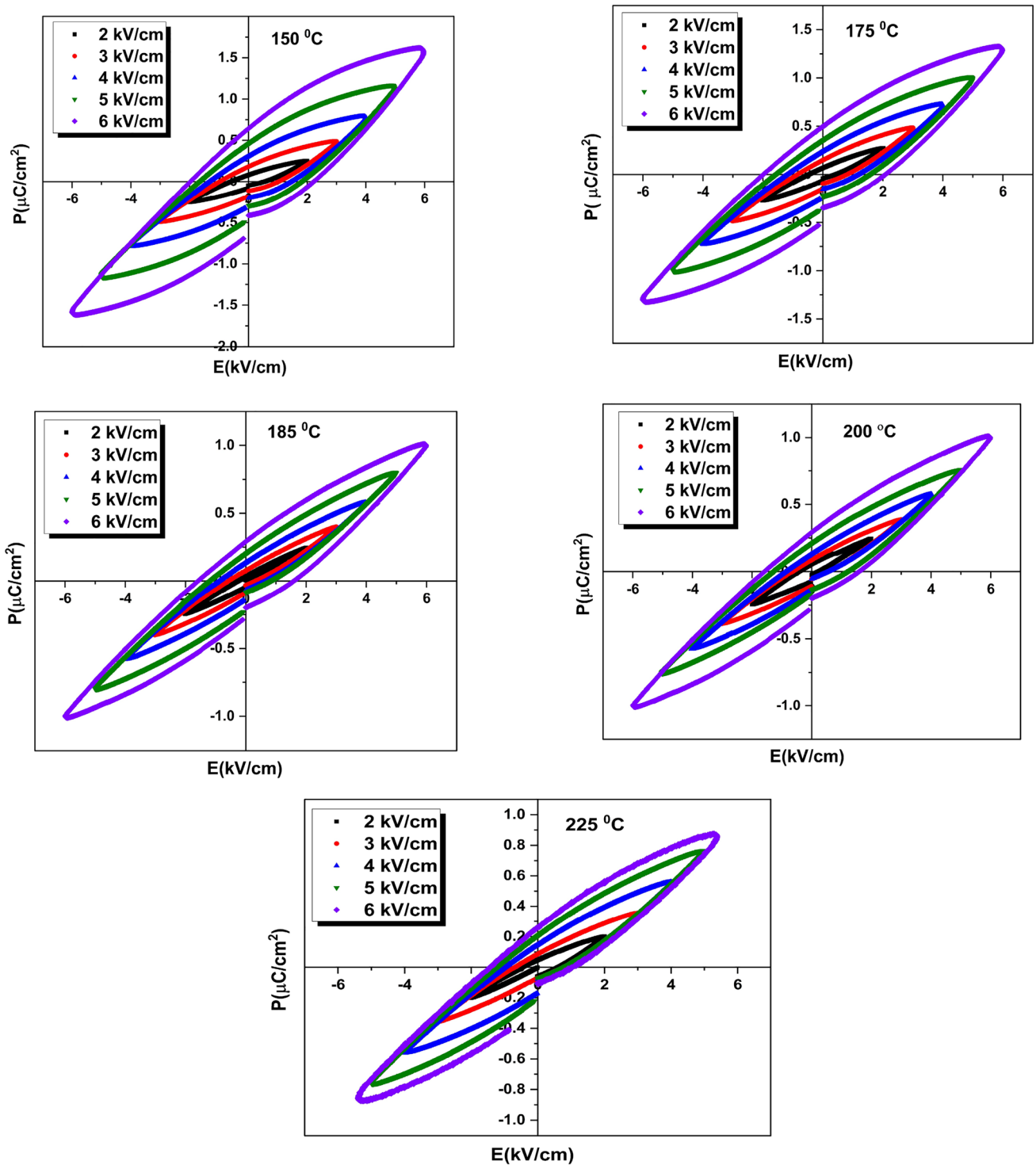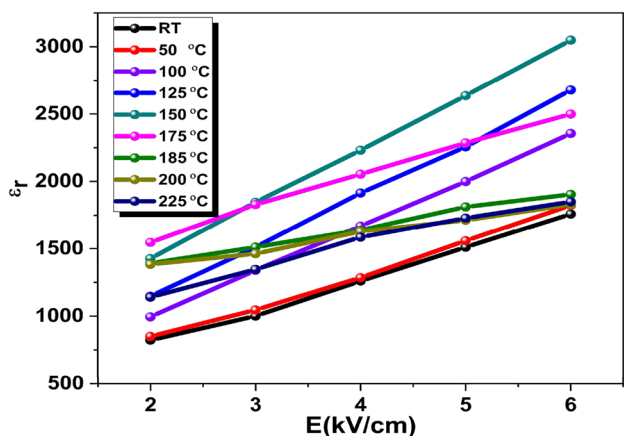
Fig. 4 (continued)

Fig. 5 Dielectric permittivity ε (E_0) as a function of electric field (E_0) amplitude for KNLNS samples under various electric field amplitudes

at high temperature is attribute to retraction of the domain size caused by the domain motion effect. While decreasing the domain switching current by increasing temperature could be related to dilution of the degree of orthorhombic phase and as consequently increase of the crystal lattice symmetry. As shown in Fig. 8, above 150 °C, we can observe that the remnant polarization and the coercive field

increases attributed to the great value of domain switchability at higher temperature [32]. In contrast, the conductivity current at high applied field was observed to be increased by the temperature increase of above 225 °C. This could be attributed to the high leakage current and dielectric loss values at high temperature (Fig. 9), due to the dependence of spontaneous polarization, Ps, dielectric permittivity loss and conductivity of ferroelectric materials on temperature [33].

4 Conclusion

In conclusion, $(K_{0.5}Na_{0.5}NbO_3)$-$0.02(LiSbO_3)$ (KNN-LS) lead-free ceramic was synthesized by solid-state sintering technique. The maximum values of permittivity peaks are attributed to (O–T) at PPT and (T–C) at Curie temperature. Rayleigh analysis shows the largest permittivity value at polymorphic phase transition and is attributed to the largest value of extrinsic contributions caused by the domain growth effect. Ferroelectric properties dependent on various temperatures show increase in the coercive field, dielectric loss and leakage current at high temperature. Based on the present results, material is a suitable candidate for energy storage application due to the large remnant polarization and low coercive field below PPT.
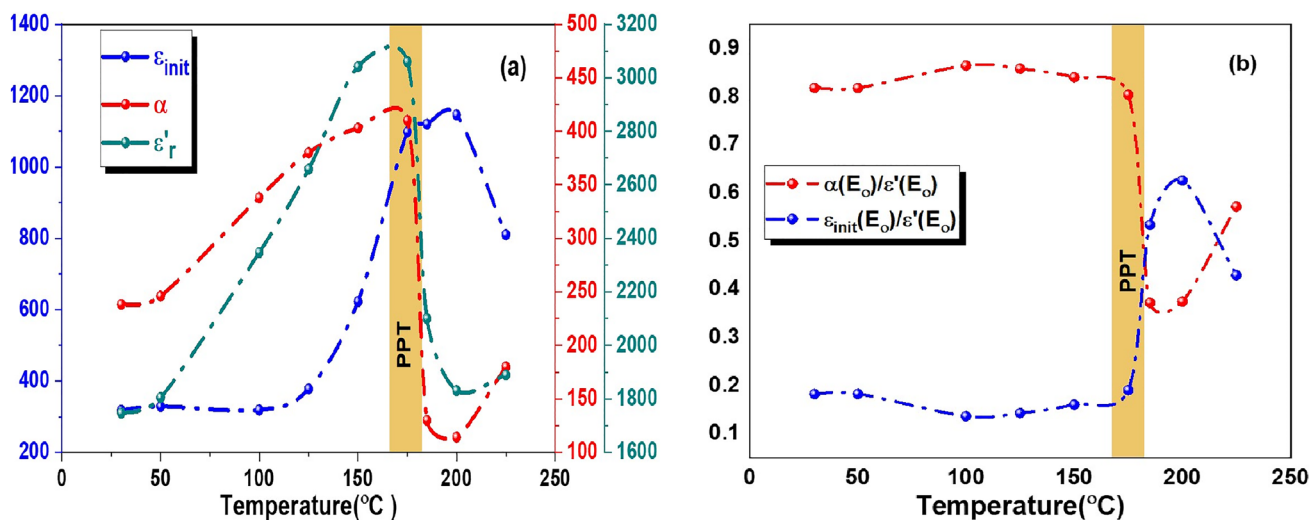

Fig. 6 **a** The initial dielectric permittivity (ε_{init}), the dielectric Rayleigh coefficient (α) and total permittivity $\varepsilon'(E_0)$. **b** The ratio $\alpha.E_0/\varepsilon'(E_0)$ (irreversible contribution) and the ratio $\varepsilon_{init}(E_0)/\varepsilon'(E_0)$ (reversible contribution) for KNN-0.02LS ceramics
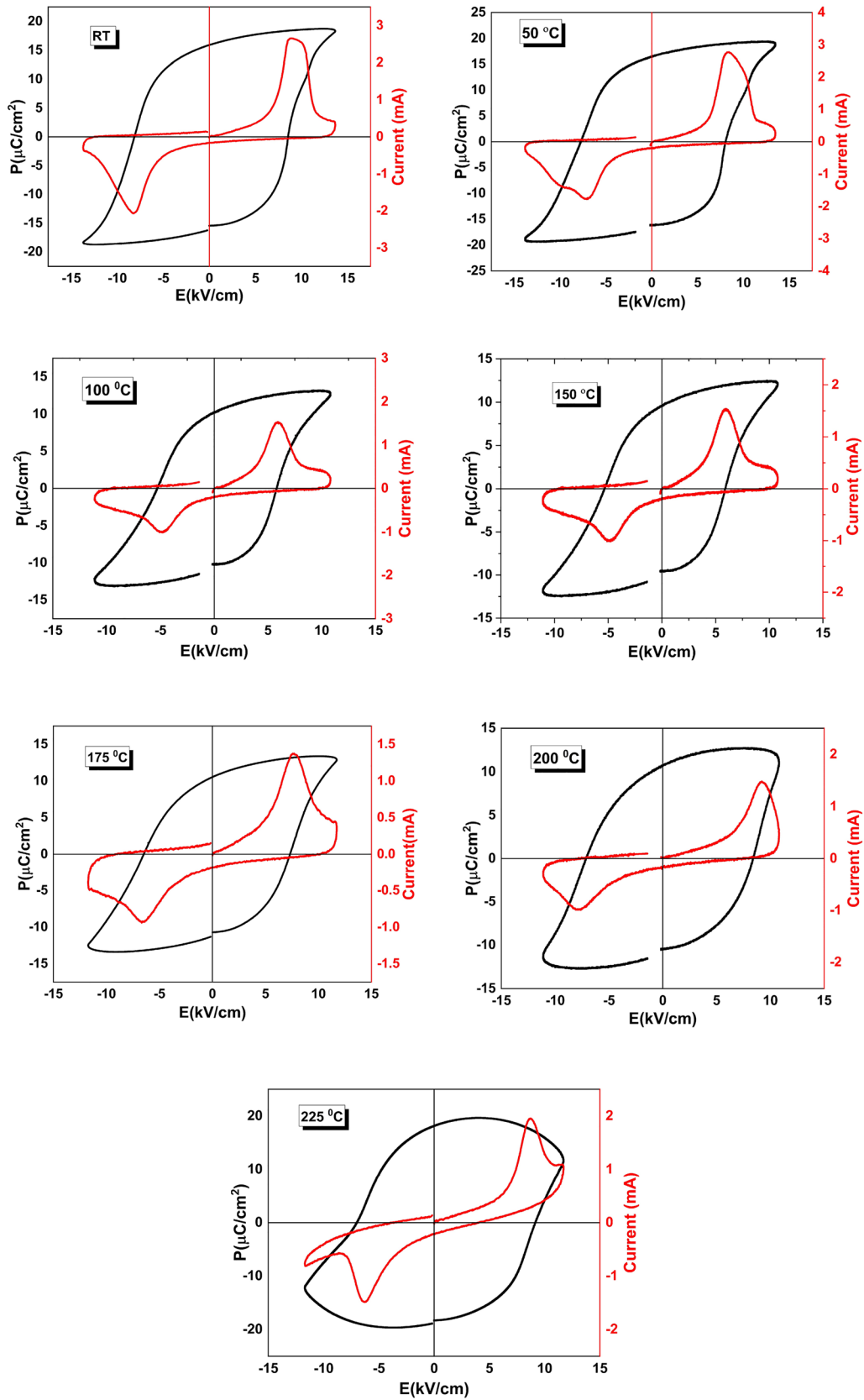
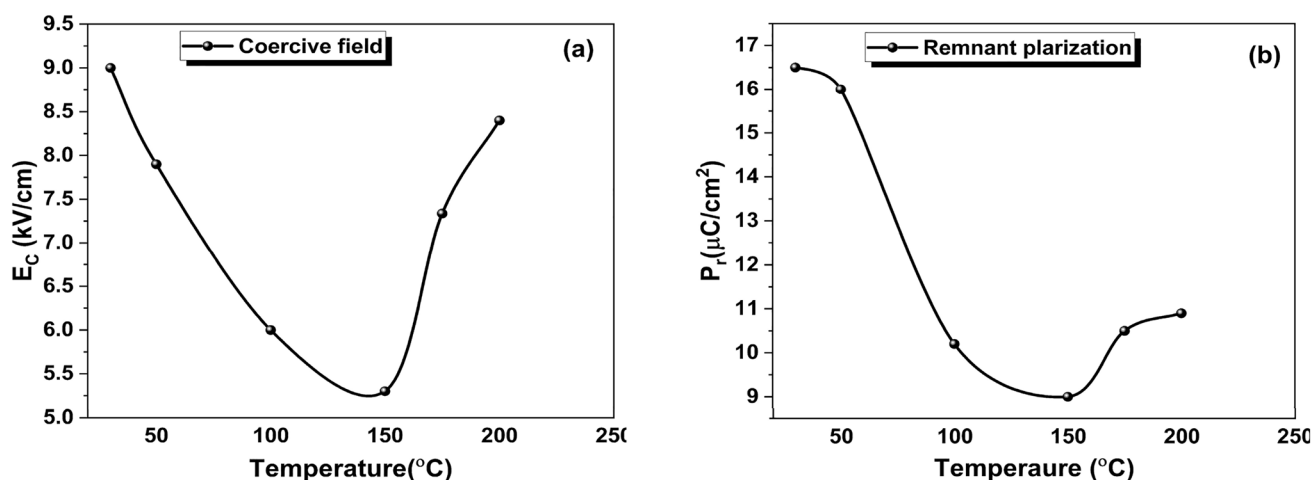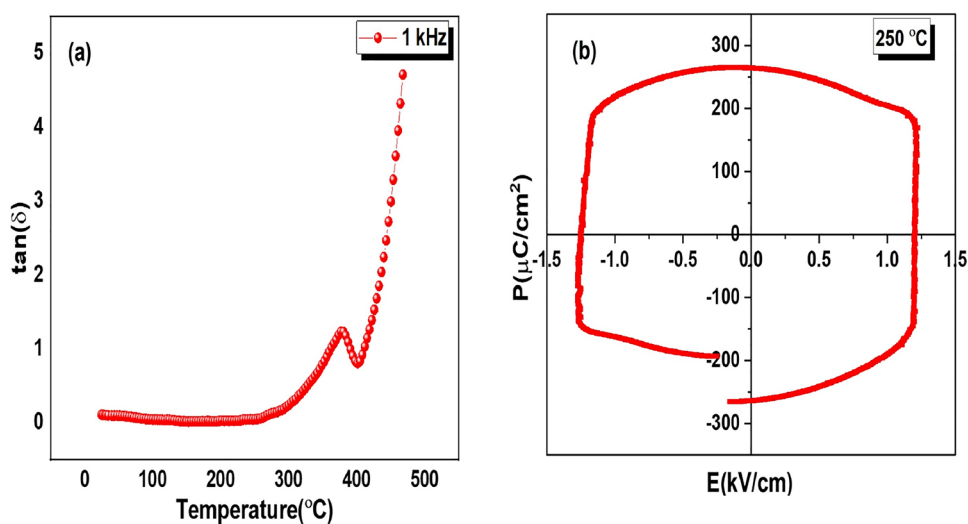**Fig. 7** The temperature dependence of P(E) hysteresis loops and I(E) loops for KNN-LS ceramic

Fig. 8 The temperature dependence of: **a** remnant polarization P_r, **b** Coercive field E_C for KNN-LS ceramic

Fig. 9 **a** Dielectric loss of KNN-LS as function of temperature. **b** P–L Loop of KNN-LS at 250 °C

Declarations

Conflict of interest The authors declare that they have no conflict of interest.

References

1. T.R. Shrout, S.J. Zhang, Lead-free piezoelectric ceramics: alternatives for PZT? J. Electroceramics. **19**, 111–124 (2007). https://doi.org/10.1007/s10832-007-9047-0

2. A.E. Mahmouda, M. Ezzeldien, S.K.S. Parashar, Enhancement of switching/un-switching leakage current and ferroelectric properties appraised by PUND method of (Ba1-xCax)TiO3 lead free piezoelectric near MPB. Solid State Sci. **93**, 44–54 (2019). https://doi.org/10.1016/j.solidstatesciences.2019.04.011

3. J. Du, Z. Xu, R. Chu, J. Hao, W. Li, G. Jiang, P. Zheng, Rare-earth doped (K0.5Na0.5)NbO3 multifunctional ceramics. J. Mater. Sci. Mater. Electron. **28**, 5288–5294 (2017). https://doi.org/10.1007/s10854-016-6186-6

4. H. Wang, X. Zhai, J. Xu, L. Yang, Effect of Sintering time on structure and properties in CuO-doping KNN-LS-BF piezoelectric ceramics. J. Wuhan Univ. Technol. Mater. Sci. Ed. **34**, 308–311 (2019). https://doi.org/10.1007/s11595-019-2052-8

5. W. Shi, J. Du, Y. Zhai, C. Chen, Y. Wei, W. Li, J. Hao, P. Fu, Intrinsic and extrinsic dielectric contributions to the electrical properties in CaZrO3-doped KNN-based electrical/optical multifunctional ceramics. J. Mater. Sci. **55**, 5741–5749 (2020). https://doi.org/10.1007/s10853-020-04444-6

6. A.E. Mahmoud, S.K.S. Parashar, Effect of domain switching contribution on polarization current, leakage current and switching charge density studied by PUND method in (Ba1−x, Cax)TiO3 ceramics. J. Mater. Sci. Eng. B. **246**, 13–20 (2019). https://doi.org/10.1016/j.mseb.2019.05.022

7. Y. Long Su, X. Ming Chen, Z. de Yu, H. Li Lian, D. di Zheng, J. Hong Peng, Comparative study on microstructure and electrical properties of (K05Na05)NbO3 lead-free ceramics prepared via two different sintering methods. J. Mater. Sci. **52**, 2934–2943 (2017). https://doi.org/10.1007/s10853-016-0587-z

8. J. Fuentes, J. Portelles, M.D. Durruthy-Rodríguez, H. H'Mok, O. Raymond, J. Heiras, M.P. Cruz, J.M. Siqueiros, Dielectric and piezoelectric properties of the KNN ceramic compound doped with Li, La and Ta. Appl. Phys. A Mater. Sci. Process. **118**, 709–715 (2015). https://doi.org/10.1007/s00339-014-8783-7

9. M. Chandrasekhar, P. Kumar, Synthesis and characterizations of SrTiO3 modified BNT-KNN ceramics for energy storage applications. J. Electroceramics. **38**, 111–118 (2017). https://doi.org/10.1007/s10832-017-0074-1

10. P. Bharathi, K.B.R. Varma, Effect of the addition of B2O3 on the density, microstructure, dielectric, piezoelectric and ferroelectric properties of K 0.5Na0.5NbO3 ceramics. J. Electron. Mater. **43**, 493–505 (2014). https://doi.org/10.1007/s11664-013-2939-7

11. Y. Guo, F. Gao, J. Xu, Q. Chen, S. Cao, L. Li, Fabrication and properties of (K0.52Na0.48)NbO3–KSr2Nb5O15 lead-free ferroelectric composite ceramics. J. Mater. Sci. Mater. Electron. **29**, 12503–12511 (2018). https://doi.org/10.1007/s10854-018-9369-5

12. T.A. Duong, C.W. Ahn, B.W. Kim, M.R. Bafandeh, H.S. Han, J.S. Lee, Effects of SrTiO3 modification on the piezoelectric and strain properties of lead-free K0.5Na0.5NbO3-based ceramics. J. Electron. Mater. **51**, 1490–1497 (2022). https://doi.org/10.1007/s11664-021-09420-7

13. H.W. Zhu, X.J. Wang, D.Y. Zheng, Z.H. Peng, L. Yang, C. Fang, Influence of BiFeO3 doping on structural and electrical properties of KNN–LS based lead-free piezoceramics. J. Mater. Sci. Mater. Electron. **29**, 13842–13851 (2018). https://doi.org/10.1007/s10854-018-9515-0

14. A.E. Mahmoud, A.S. Afify, S.K.S. Parashar, Dielectric, tunability, leakage current, and ferroelectric properties of (K0.45Na0.55)0.95Li005NbO3 lead free piezoelectric. J. Mater. Sci. Mater. Electron. (2019). https://doi.org/10.1007/s10854-018-0542-7

15. J. Chen, J. Cheng, J. Guo, Z. Cheng, J. Wang, H. Liu, S. Zhang, Excellent thermal stability and aging behaviors in BiFeO3-BaTiO3 piezoelectric ceramics with rhombohedral phase. J. Am. Ceram. Soc. **103**, 374–381 (2020). https://doi.org/10.1111/jace.16755

16. Z. Yang, Y. Chang, B. Liu, L. Wei, Effects of composition on phase structure, microstructure and electrical properties of (K0.5Na0.5)NbO3-LiSbO3 ceramics. Mater. Sci. Eng. A. **432**, 292–298 (2006). https://doi.org/10.1016/j.msea.2006.06.034

17. L.M. Zheng, J.F. Wang, C.M. Wang, Q.Z. Wu, G.Z. Zang, Thermal stability and humidity resistance of ScTaO4 modified (K0.5Na0.5)NbO3 ceramics. Chinese Phys. Lett. **26**, 4 (2009). https://doi.org/10.1088/0256-307X/26/12/127701

18. J. Gao, X. Hu, L. Zhang, F. Li, L. Zhang, Y. Wang, Y. Hao, L. Zhong, X. Ren, Major contributor to the large piezoelectric response in (1–x)Ba(Zr0.2Ti0.8)O3–x(Ba0.7Ca0.3)TiO3 ceramics: domain wall motion. Appl. Phys. Lett. **104**, 252909 (2014). https://doi.org/10.1063/1.4885675

19. R.E. Eitel, T.R. Shrout, C.A. Randall, Nonlinear contributions to the dielectric permittivity and converse piezoelectric coefficient in piezoelectric ceramics. J. Appl. Phys. (2006). https://doi.org/10.1063/1.2207738

20. D. Kim, Nonlinearity in piezoelectric ceramics. J. Mater. Sci. **6**, 4575–4601 (2002)

21. A.E. Mahmoud, A.M. Babeer, Intrinsic and extrinsic contributions in nonlinear dielectric response of (Bi0.5Na0.3K0.2)TiO3-(Ba0.8Ca0.2)TiO3—based SrTiO3 ceramics driven by the Rayleigh Model. J. Electron. Mater. (2021). https://doi.org/10.1007/s11664-021-09303-x

22. A.B. Haugen, M.I. Morozov, J.L. Jones, M.A. Einarsrud, Rayleigh analysis of dielectric properties in textured K0.5Na0.5NbO3 ceramics. J. Appl. Phys. **116**, 10–15 (2014). https://doi.org/10.1063/1.4902858

23. B. Peng, Z. Yue, L. Li, Evaluation of domain wall motion during polymorphic phase transition in (K, Na)NbO3-based piezoelectric ceramics by nonlinear response measurements. J. Appl. Phys. (2011). https://doi.org/10.1063/1.3553857

24. T.A. Skidmore, T.P. Comyn, S.J. Milne, Temperature stability of ([Na0.5K0.5NbO3] 0.93-[LiTaO3]0.07) lead-free piezoelectric ceramics. Appl. Phys. Lett. **94**, 7–11 (2009). https://doi.org/10.1063/1.3153157

25. J. Kim, J.H. Ji, D.J. Shin, J.H. Koh, Improved Li and Sb doped lead-free (Na, K)NbO3 piezoelectric ceramics for energy harvesting applications. Ceram. Int. **44**, 22219–22224 (2018). https://doi.org/10.1016/j.ceramint.2018.08.341

26. R. Gaur, K.C. Singh, R. Laishram, Dependence of dielectric properties on sintering conditions of lead free KNN ceramics modified with Li-Sb. World Acad. Sci. Eng. Technol. **9**, 768–771 (2015)

27. Z. Yang, H. Du, S. Qu, Y. Hou, H. Ma, J. Wang, J. Wang, X. Wei, Z. Xu, Significantly enhanced recoverable energy storage density in potassium-sodium niobate-based lead free ceramics. J. Mater. Chem. A. **4**, 13778–13785 (2016). https://doi.org/10.1039/c6ta04107h

28. Y. Huan, X. Wang, L. Li, J. Koruza, Strong domain configuration dependence of the nonlinear dielectric response in (K, Na)NbO3-based ceramics. Appl. Phys. Lett. (2015). https://doi.org/10.1063/1.4936165

29. Z. Wang, R. Zhang, E. Sun, W. Cao, Contributions of domain wall motion to complex electromechanical coefficients of 0.62Pb(Mg1/3Nb2/3)O3–0.38PbTiO3 crystals. J. Appl. Phys. **107**, 4 (2010). https://doi.org/10.1063/1.3273484

30. Q.M. Zhang, W.Y. Pan, S.J. Jang, L.E. Cross, Domain wall excitations and their contributions to the weak-signal response of doped lead zirconate titanate ceramics. J. Appl. Phys. **64**, 6445–6451 (1988). https://doi.org/10.1063/1.342059

31. N. Tsutsumi, K. Okumachi, K. Kinashi, W. Sakai, Re-evaluation of the origin of relaxor ferroelectricity in vinylidene fluoride terpolymers: an approach using switching current measurements. Sci. Rep. **7**, 1–8 (2017). https://doi.org/10.1038/s41598-017-16017-w

32. Y. Sratta, S. Chandarak, M. Unruan, P. Kantha, B. Marungsri, R. Yimnirun, S. Pojprapai, Effect of temperature on ferroelectric properties of bismuth ferrite-barium titanate. Integr. Ferroelectr. **148**, 67–72 (2013). https://doi.org/10.1080/10584587.2013.852027

33. H. Khelifi, I. Zouari, A. Al-Hajry, N. Abdelmoula, D. Mezzane, H. Khemakhem, Ac conductivity and ferroelectric phase transition of Bi0.7(Ba0.8Sr0.2)0.3Fe0.7Ti0.3O3 ceramic. Ceram. Int. **41**, 12958–12966 (2015). https://doi.org/10.1016/j.ceramint.2015.06.139